

Study of Support Motion of a Finite Bar with a Boundary Damper and a Spring Using Analytical Approaches and FEM

Jeng-Tzong Chen ^{*,†,‡,§,||}, Hao-Chen Kao^{*}, Jia-Wei Lee ^{¶,**} and Ying-Te Lee^{*}

^{*}*Department of Harbor and River Engineering
National Taiwan Ocean University, Keelung, Taiwan*

[†]*Department of Mechanical and Mechatronic Engineering
National Taiwan Ocean University, Keelung, Taiwan*

[‡]*Department of Civil Engineering
National Taiwan University, Taipei, Taiwan*

[§]*Department of Civil Engineering
National Cheng Kung University, Tainan, Taiwan*

[¶]*Department of Civil Engineering
Tamkang University, New Taipei City, Taiwan*

^{||}*jtchen@mail.ntou.edu.tw*
^{**}*152734@mail.tku.edu.tw*

Received 19 December 2023

Accepted 21 February 2024

Published 27 March 2024

In this paper, we solve the vibration problem of a finite bar with a viscously damped boundary in conjunction with a spring on the same side subject to the support motion on the other side. To avoid the computation of complex modes and the difficulty of orthogonal conditions for the partial differential equation (PDE) of a continuous system, two alternatives are employed. One is the analytical derivation by using the diamond rule of the method of characteristics. The advantage is that this method can yield an analytical solution. However, the disadvantage is that the method can be only applied to some simple problems such as a linear system and the one-dimensional (1D) wave equation. The other numerical method, finite element method (FEM), is incorporated into a general-purpose program to solve this problem. The advantage of the FEM is that this methodology can be applied to solve various problems such as different PDEs. Therefore, the solution obtained by using the FEM is compared with that of the analytical solution. Two special cases, only a spring and a damper alone, are also considered by using the FEM. Interestingly, the same silent area is captured in the displacement profile by using the FEM for the three cases. We also find that the displacement profiles have slope discontinuity which only occurs on the characteristic line. After the wave front arrives at the boundary, various responses appear due to different boundaries, spring, damper

^{||,**}Corresponding authors.

and both. It is found that the displacement amplitude of the general case is smaller than the other two special cases. This result matches the application of engineering practice.

Keywords: Support motion; viscous damper; spring; finite element method; diamond rule.

1. Introduction

Since wave propagation as well as dynamic vibration occur in engineering mechanics and physics, various problems are always modeled by using the wave equation, e.g. support motion problem of earthquake engineering. In the engineering practice, real problems for buildings, plate, beam, cars and equipment were solved by using the partial differential equation (PDE) model subjected to the support motion. Many researchers have investigated this problem by using various methods, e.g. the mode superposition technique,¹ the method of separation variables,²⁻⁴ the method of quasi-static decomposition,⁴⁻⁷ the method of the diamond rule^{4-6,8} or the so-called method of characteristics, the image method,⁸ the finite element method (FEM),⁹⁻¹¹ the boundary element method (BEM)¹² and the meshless method,^{13,14} etc.

Hull² and Jovanovic¹⁵ solved vibration problems of bar and beam with a viscous boundary, respectively. A non-self-adjoint operator and orthogonality condition of complex modes need special care. Jovanovic¹⁶ extended an axial damping to a torsion damper. Dampers at both ends were also investigated and stability condition was also discussed by Udewadia¹⁷ and Jovanovic.¹⁸ A beam including the internal damping in the span and a boundary damper was studied by Gurgoze and Erol.¹⁹ Since a viscous damper is always considered to reduce the vibration response, the support motion of earthquake engineering is the main concern of this paper. Analytical solutions for a system with an external damper and spring are sparse. Results of continuous and discrete systems were compared with those by Singh *et al.*³ Besides, a case of limiting damping was also discussed. Although Hull² claimed that he derived a closed-form solution and compared it with FEM well, the solution was a series form instead of a closed form. In addition, he showed only a frequency-domain example subject to a concentrated dynamic loading. Chen *et al.*^{5,6} employed the method of characteristics and the mode superposition approach in conjunction with the quasi-static decomposition technique to revisit the problem subject to the support motion instead of the forced excitation.

D'Alembert's solution provides an exact expression of displacement for an infinite string with arbitrary initial displacement and velocity. Method of characteristics, also named the diamond rule, can be found in the textbook of Farlow.²⁰ It is popularly employed to solve various kinds of problems, e.g. water hammer.²¹ The diamond rule using D'Alembert's solution was proposed by John²² in 1975 and was always used to solve the wave problem. An exact solution of an infinite string with a mass, a damper and a spring at the origin subject to the initial displacement was derived and animation was also made.⁸ Recently, Xing and Sun²³

studied the multi-objective optimization of the viscous boundary damper of an elastic rod by employing a hybrid method of a genetic algorithm and simple cell mapping (GA-SCM). Green's function of the impulse response of an elastic rod with a lumped mass and damper-spring termination was also studied using Lagrange's method by Xing and Sun.²⁴ Two parts, one satisfying homogeneous boundary condition (B. C.) and the other particular solution satisfying non-homogeneous B. C. were derived. To the authors' best knowledge, the vibration problem of a bar with both the spring and damper subjected to support motion was not analytically and numerically solved although a single spring or a damper alone was done before. Providing the exact solution for the problem is the innovation of this paper. Besides, we also provided the numerical result to check the validity of our analytical solution by using the FEM.

In this paper, we extended the finite bar with an external spring⁵ or a viscously damped boundary⁶ to both a spring and a viscous damper together. Two methods, analytical (the method of characteristics) and numerical (FEM) approaches, were employed to solve the problem. The comparison of the result between continuous and discrete systems was also done. For the two special cases of only a spring and only a viscous damper, the silent area or the so-called dead zone in the time-space plane separated by characteristic lines to several regions was also examined for three approaches, the method of characteristics,^{5,6} the mode superposition method^{5,6} and the FEM. Besides, the slope discontinuity of the displacement profile is also our concern to discuss where it appears in the time-space domain.

2. Problem Statements and Methods of Solution

We extend our previous experience^{5,6} to solve the vibration problem of a finite bar with a viscous damper and a spring boundary subject to the support motion at the other end, as shown in Fig. 1. Here, a finite bar with a viscous damper and a spring on the right boundary is considered at the same time. The axial displacement field of a finite bar, $u(x, t)$, satisfies the following equation:

$$c^2 \frac{\partial^2 u(x, t)}{\partial x^2} = \frac{\partial^2 u(x, t)}{\partial t^2}, 0 < x < L, t > 0, \quad (1)$$

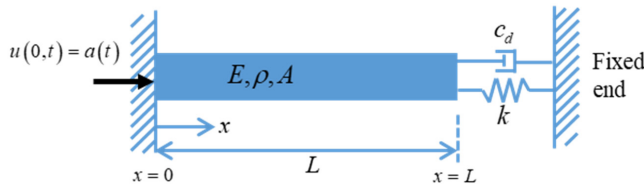


Fig. 1. A finite bar with a viscous damper and a spring at the right end of $x = L$, subjected to a support motion at $x = 0$.

where $c = \sqrt{EA/\rho}$ and $u(x, t)$ denote the wave speed and displacement in the x -direction at the time t , respectively. The symbols E, A, ρ and L denote Young's modulus, the area of cross-section, the mass per unit length and the length of the bar, respectively. The initial displacement $\phi(x)$ and the initial velocity $\varphi(x)$ conditions are, respectively, given by

$$u(x, t)|_{t=0} = \phi(x), \tag{2}$$

$$\frac{\partial u(x, t)}{\partial t} \Big|_{t=0} = \varphi(x). \tag{3}$$

Here, we start from the rest condition that $\phi(x)$ and $\varphi(x)$ are both equal to zero.

The time-dependent B. C. at the left-hand side ($x = 0$) of the finite bar is given by the specified support motion as follows:

$$u(0, t) = a(t). \tag{4}$$

The B. C. at the right-hand side due to a viscous damper and a spring (at the end $x = L$) is given as follows:

$$EA \frac{\partial u(x, t)}{\partial x} \Big|_{x=L} = -c_d \frac{\partial u(x, t)}{\partial t} \Big|_{x=L} - ku(x, t)|_{x=L}, \tag{5}$$

where c_d and k denote the damping coefficient and the spring constant, respectively, as shown in Fig. 1.

2.1. Diamond rule based on the method of characteristics

The general solution of one-dimensional (1D) wave equation of the second-order PDE can be derived by using the method of characteristic line as follows:

$$u(x, t) = P(x + ct) + Q(x - ct), \tag{6}$$

where $P(x + ct)$ and $Q(x - ct)$ denote a left-going-traveling wave and a right-going-traveling wave, respectively. By plotting two characteristic lines, $x + ct = nL, n = 0, 1, 2, \dots$ and $x - ct = -nL, n = 0, 1, 2, \dots$, the space-time domain is decomposed into several regions (regions I, II, III ...), as shown in Fig. 2(a). Each region in Fig. 2(a) is a parallelogram or an isosceles triangle. After using Eq. (6) to satisfy the initial conditions (I.C.s) in Eqs. (2) and (3), we have D'Alembert's solution for region I (blue region in Fig. 2(a)),

$$u(x, t) = \frac{1}{2}[\phi(x + ct) + \phi(x - ct)] + \frac{1}{2c} \int_{x-ct}^{x+ct} \varphi(\tau) d\tau, \quad (x, t) \in \text{I}, \tag{7}$$

where $\phi(\cdot)$ and $\varphi(\cdot)$ are initial displacement and velocity, respectively. According to the property of D'Alembert's solution, we have the relationship for the displacements at four vertices (A, B, C and D) of a diamond as shown as follows:

$$u_A + u_B = u_C + u_D, \tag{8}$$

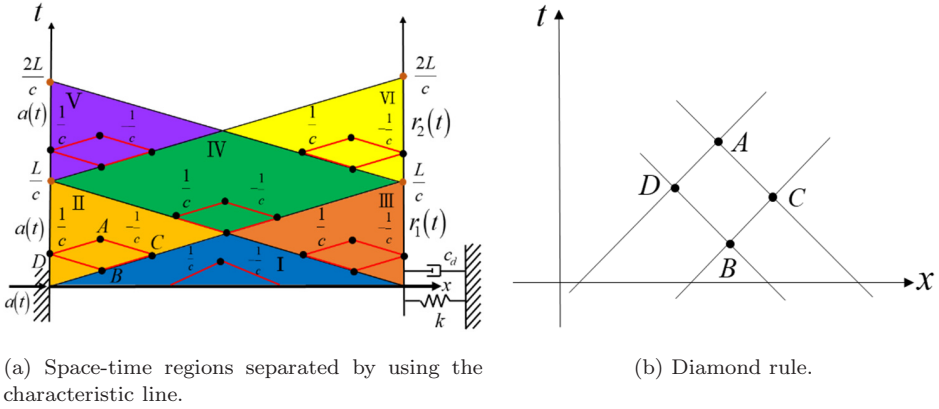


Fig. 2. Method of characteristics and diamond rule.

where u_A, u_B, u_C and u_D denote the displacement at the four points A, B, C and D , respectively, as shown in Fig. 2(b). It is noted that any side of a diamond is parallel to a certain characteristic line. Equation (8) is the so-called diamond rule.^{4-6,8} We employ the space-time marching scheme in Eq. (8) to obtain the displacement response for the successive regions of any time and space. By using the diamond rule for the former six regions as shown in Fig. 2(a), the displacements are expressed as follows:

$$u_I(x, t) = 0, \quad (x, t) \in \text{I}, \quad (9)$$

$$u_{II}(x, t) = a \left(\frac{ct - x}{c} \right), \quad (x, t) \in \text{II}, \quad (10)$$

$$u_{III}(x, t) = r_1 \left(\frac{x + ct - L}{c} \right), \quad (x, t) \in \text{III}, \quad (11)$$

$$u_{IV}(x, t) = a \left(\frac{ct - x}{c} \right), \quad (x, t) \in \text{IV}, \quad (12)$$

$$u_V(x, t) = a \left(\frac{ct - x}{c} \right), \quad (x, t) \in \text{V}, \quad (13)$$

$$u_{VI}(x, t) = a \left(\frac{ct - x}{c} \right) - a \left(\frac{x + ct - 2L}{c} \right) + r_2 \left(\frac{x + ct - L}{c} \right), \quad (x, t) \in \text{VI}, \quad (14)$$

where $r_1(t)$ and $r_2(t)$ stand for the displacements of $u(L, t), 0 \leq t \leq L/c$ and $u(L, t), L/c \leq t \leq 2L/c$, respectively. For the displacement in the other time-space region, it can be obtained by using the iterative procedure of the time-space marching scheme. Since the boundary displacement at the end of the right-hand side is

unknown, it is necessary to assume two unknown functions ($r_1(t)$ and $r_2(t)$) on the right-hand side boundary of the full time-space region. After using the corresponding displacement representation for regions III and VI to satisfy the B. C. in Eq. (5), we have

$$EA \frac{\partial u_{III}(x, t)}{\partial x} \Big|_{x=L} = -c_d \frac{\partial u_{III}(x, t)}{\partial t} \Big|_{x=L} - k u_{III}(x, t)|_{x=L}, \quad 0 \leq t \leq L/c, \quad (15)$$

$$EA \frac{\partial u_{VI}(x, t)}{\partial x} \Big|_{x=L} = -c_d \frac{\partial u_{VI}(x, t)}{\partial t} \Big|_{x=L} - k u_{VI}(x, t)|_{x=L}, \quad L/c \leq t \leq 2L/c, \quad (16)$$

where $u_{III}(x, t)$ and $u_{VI}(x, t)$ denote the displacement function in regions III and VI, respectively.

Thus, we solve $r_1(t)$ by using Eq. (11) to satisfy Eq. (15). The displacement at $x = L$, $u_{III}(L, 0)$ and $u_I(L, 0)$, must satisfy the displacement continuity. Then, we have

$$r_1(t) = 0, 0 \leq t \leq L/c, \quad (17)$$

since the wave front information has not arrived yet.

Similarly, the solution of $r_2(t)$ is derived by using Eq. (14) to satisfy Eq. (16). By solving the corresponding first-order ordinary differential equation (ODE) for $r_2(t)$ at the end of spring and damper as shown as follows:

$$r_2'(t) + \frac{kc}{EA + c_d c} r_2(t) = \frac{2EA}{EA + c_d c} a' \left(\frac{ct - L}{c} \right), \quad L/c \leq t \leq 2L/c, \quad (18)$$

we obtain

$$r_2(t) = e^{-\frac{kc}{AE+c_d c} t} \int^t e^{\frac{kc}{AE+c_d c} \tau} \cdot \frac{2EA}{EA + c_d c} a' \left(\frac{c\tau - L}{c} \right) d\tau, \quad L/c \leq t \leq 2L/c, \quad (19)$$

after using the integrating factor, where the undetermined constant is determined by satisfying the displacement continuity in regions IV and VI at $(x, t) = (L, L/c)$, as shown in Fig. 2(a).

2.2. FEM

For the discrete system of FEM with uniformly distributed N degrees-of-freedom of a bar as shown in Fig. 3, we consider the following equation:

$$[M]\{\ddot{U}\} + [C]\{\dot{U}\} + [K]\{U\} = \{P\}, \quad (20)$$

where $[M]$, $[C]$ and $[K]$ are the mass, damping and stiffness matrices, respectively, all being square matrices of dimension N , the total number of degrees-of-freedom, $\{U\}$ is the nodal displacement and $\{P\}$ is the nodal force, all being column vectors of N by 1. We decompose the degrees-of-freedom into two sets, the supported and the unsupported, denoted by the subscripts r and l , respectively. By separating

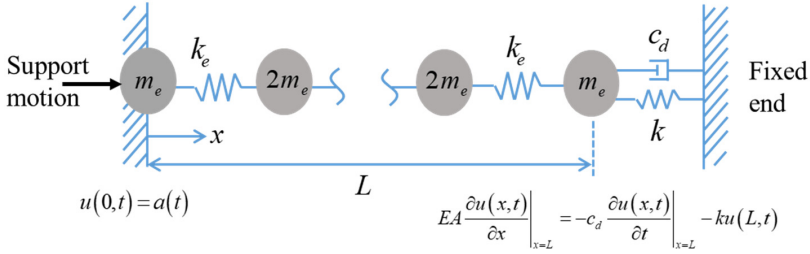


Fig. 3. A FEM model of discrete system for a finite bar with N degrees-of-freedom.

the supported (r) and unsupported (l) sets for the displacement, Eq. (20) can be rewritten as

$$\begin{bmatrix} M_{rr} & M_{rl} \\ M_{lr} & M_{ll} \end{bmatrix} \begin{Bmatrix} \ddot{U}_r \\ \ddot{U}_l \end{Bmatrix} + \begin{bmatrix} C_{rr} & C_{rl} \\ C_{lr} & C_{ll} \end{bmatrix} \begin{Bmatrix} \dot{U}_r \\ \dot{U}_l \end{Bmatrix} + \begin{bmatrix} K_{rr} & K_{rl} \\ K_{lr} & K_{ll} \end{bmatrix} \begin{Bmatrix} U_r \\ U_l \end{Bmatrix} = \begin{Bmatrix} P_r \\ P_l \end{Bmatrix}, \quad (21)$$

where $\{U_r\}$ prescribes N_r support motions, $\{P_r\}$ contains the resulting N_r reaction forces, $\{P_l\}$ prescribes N_l nodal loads and $\{U_l\}$ contains the resulting N_l nodal displacements, where $N_r + N_l = N$. Since we focus on support motion problems in earthquake engineering, the N_r entries of $\{U_r\}$ are prescribed by time histories at N_r supports and it is assumed that $\{P_l\} = \{0\}$. The discrete system of the case in Fig. 3 is only a single support. Therefore, $N_r = 1$, is considered.

The solution, $\{U\}$ and the nodal force, $\{P\}$, can be decomposed into two parts. One is the quasi-static part with the superscript s , the other is the dynamic-inertia part with the superscript d . They are shown as follows:

$$\{U\} = \begin{Bmatrix} U_r \\ U_l \end{Bmatrix} = \{U^s\} + \{U^d\} = \begin{Bmatrix} U_r^s \\ U_l^s \end{Bmatrix} + \begin{Bmatrix} U_r^d \\ U_l^d \end{Bmatrix} \quad (22)$$

and

$$\{P\} = \begin{Bmatrix} P_r \\ P_l \end{Bmatrix} = \{P^s\} + \{P^d\} = \begin{Bmatrix} P_r^s \\ P_l^s \end{Bmatrix} + \begin{Bmatrix} P_r^d \\ P_l^d \end{Bmatrix}. \quad (23)$$

For the dynamic-inertia part, we have

$$\{P_l^d\} = \{0\}, \quad (24)$$

$$\{U_r^d\} = \{0\}. \quad (25)$$

According to the assumption $\{P_l\} = 0$, we have

$$\{P_l^s\} = \{0\}. \quad (26)$$

From the force equilibrium for the FEM model of Fig. 3, we construct the mass, damping and stiffness matrices as shown as follows:

$$\begin{aligned}
 [M] &= \begin{bmatrix} m_e & 0 & 0 & \cdots & 0 \\ 0 & 2m_e & 0 & \ddots & \vdots \\ 0 & 0 & \ddots & 0 & 0 \\ \vdots & \ddots & 0 & 2m_e & 0 \\ 0 & \cdots & 0 & 0 & m_e \end{bmatrix}_{N \times N}, & [C] &= \begin{bmatrix} 0 & \cdots & 0 \\ \ddots & & \\ \vdots & \ddots & \vdots \\ 0 & \cdots & 0 & c_d \end{bmatrix}_{N \times N}, \\
 [K] &= \begin{bmatrix} k_e & -k_e & 0 & \cdots & 0 \\ -k_e & 2k_e & -k_e & \ddots & \vdots \\ 0 & -k_e & \ddots & \ddots & 0 \\ \vdots & \ddots & \ddots & 2k_e & -k_e \\ 0 & \cdots & 0 & -k_e & k_e + k \end{bmatrix}_{N \times N}, & & (27)
 \end{aligned}$$

where k_e denotes the equivalent spring constant of bar element, $k_e = EA(N - 1)/L$ and m_e denotes the equivalent mass of the bar element as a mass block, $m_e = \rho L/2(N - 1)$.

Regarding the definition of the quasi-static solution, we have

$$\begin{aligned}
 &\begin{bmatrix} 0 & \cdots & 0 \\ \ddots & & \\ \vdots & \ddots & \\ 0 & \cdots & 0 & c_d \end{bmatrix} \begin{Bmatrix} \dot{U}_r^s \\ \dot{U}_{l(1)}^s \\ \dot{U}_{l(2)}^s \\ \vdots \\ \dot{U}_{l(N_l)}^s \end{Bmatrix} + \begin{bmatrix} k_e & -k_e & 0 & \cdots & 0 \\ -k_e & 2k_e & -k_e & \ddots & \vdots \\ 0 & -k_e & \ddots & \ddots & 0 \\ \vdots & \ddots & \ddots & 2k_e & -k_e \\ 0 & \cdots & 0 & -k_e & k_e + k \end{bmatrix} \begin{Bmatrix} U_r^s \\ U_{l(1)}^s \\ U_{l(2)}^s \\ \vdots \\ U_{l(N_l)}^s \end{Bmatrix} \\
 &= \begin{Bmatrix} P_r^s \\ 0 \\ 0 \\ \vdots \\ 0 \end{Bmatrix}, & & (28)
 \end{aligned}$$

where the dynamic-inertia part is neglected for the quasi-static solution.

By summing all simultaneous row equations in the algebraic equation of Eq. (28), we obtain the following equation:

$$kU_{l(N_l)}^s + c_d\dot{U}_{l(N_l)}^s = P_r^s. \tag{29}$$

Thus, Eq. (28) can be rewritten as

$$\begin{bmatrix} k_e & 0 & -k_e & 0 & \cdots & 0 \\ 0 & k_e & 0 & 0 & \ddots & -k_e \\ -k_e & 0 & 2k_e & -k_e & \ddots & 0 \\ 0 & 0 & -k_e & 2k_e & \ddots & 0 \\ \vdots & \ddots & \ddots & \ddots & \ddots & -k_e \\ 0 & -k_e & 0 & 0 & -k_e & 2k_e \end{bmatrix} \begin{Bmatrix} U_r^s \\ U_{l(N_l)}^s \\ U_{l(1)}^s \\ U_{l(2)}^s \\ \vdots \\ U_{l(N_l-1)}^s \end{Bmatrix} = \begin{Bmatrix} P_r^s \\ -P_r^s \\ 0 \\ 0 \\ \vdots \\ 0 \end{Bmatrix}. \quad (30)$$

In order to employ the Guyan reduction method, we decompose Eq. (30) into

$$k_e \begin{bmatrix} 1 & 0 & -1 & 0 & \cdots & 0 \\ 0 & 1 & 0 & 0 & \ddots & -1 \\ -1 & 0 & 2 & -1 & \ddots & 0 \\ 0 & 0 & -1 & 2 & \ddots & 0 \\ \vdots & \ddots & \ddots & \ddots & \ddots & -1 \\ 0 & -1 & 0 & 0 & -1 & 2 \end{bmatrix} \begin{Bmatrix} U_r^s \\ U_{l(N_l)}^s \\ U_{l(1)}^s \\ U_{l(2)}^s \\ \vdots \\ U_{l(N_l-1)}^s \end{Bmatrix} = \begin{Bmatrix} P_r^s \\ -P_r^s \\ 0 \\ 0 \\ \vdots \\ 0 \end{Bmatrix}. \quad (31)$$

By expanding Eq. (31), the Guyan reduction yields

$$\begin{Bmatrix} U_{l(1)}^s \\ U_{l(2)}^s \\ \vdots \\ U_{l(N_l-1)}^s \end{Bmatrix}_{(N-2) \times 1} = - \begin{bmatrix} 2 & -1 & 0 & 0 \\ -1 & 2 & \ddots & 0 \\ 0 & \ddots & \ddots & -1 \\ 0 & 0 & -1 & 2 \end{bmatrix}_{(N-2) \times (N-2)}^{-1} \times \begin{bmatrix} -1 & 0 \\ 0 & \vdots \\ \vdots & 0 \\ 0 & -1 \end{bmatrix}_{(N-2) \times 2} \begin{Bmatrix} U_r^s \\ U_{l(N_l)}^s \end{Bmatrix}_{2 \times 1}, \quad (32)$$

where U_r^s is the prescribed time history at the support side, i.e. $U_r^s = a(t)$. Each element in the column vector, $\{U_{l(1)}^s \ U_{l(2)}^s \ \cdots \ U_{l(N_l-1)}^s\}^T$, can be obtained by

U_r^s and $U_{i(N_i)}^s$. Here, we extract the N th equation in Eq. (28) to have

$$c_d \dot{U}_{i(N_i)}^s - k_e U_{i(N_i-1)}^s + (k_e + k) U_{i(N_i)}^s = 0, \quad (33)$$

where $U_{i(N_i-1)}^s$ in Eq. (33) can be represented by U_r^s and $U_{i(N_i)}^s$ in Eq. (32). Therefore, Eq. (33) reduces to a first-order ODE of $U_{i(N_i)}^s$. By solving Eq. (33), the unknown $U_{i(N_i)}^s$ can be obtained. Finally, all nodal displacements in the column vector, $\left\{ U_{i(1)}^s \quad U_{i(2)}^s \quad \cdots \quad U_{i(N_i)}^s \right\}^T$, are known.

Substituting Eqs. (22) and (23) into Eq. (21), we have

$$\begin{aligned} & \begin{bmatrix} M_{rr} & M_{rl} \\ M_{lr} & M_{ll} \end{bmatrix} \begin{Bmatrix} 0 \\ \ddot{U}_l^d \end{Bmatrix} + \begin{bmatrix} C_{rr} & C_{rl} \\ C_{lr} & C_{ll} \end{bmatrix} \begin{Bmatrix} 0 \\ \dot{U}_l^d \end{Bmatrix} + \begin{bmatrix} K_{rr} & K_{rl} \\ K_{lr} & K_{ll} \end{bmatrix} \begin{Bmatrix} 0 \\ U_l^d \end{Bmatrix} \\ & = - \begin{bmatrix} M_{rr} & M_{rl} \\ M_{lr} & M_{ll} \end{bmatrix} \begin{Bmatrix} \ddot{U}_r^s \\ \dot{U}_l^s \end{Bmatrix}, \end{aligned} \quad (34)$$

where the term in the right-hand side of equation sign is the forcing function due to the support motion.

For the finite bar of N finite nodes ($N - 1$ bar elements), the submatrices of $[M]$, $[C]$ and $[K]$ for the illustrative example of Fig. 3 are explicitly expressed as follows:

$$\begin{aligned} [M_{rr}] &= [m_e]_{N_r \times N_r}, [M_{rl}] = [0 \quad \cdots \quad 0]_{N_r \times N_l}, [M_{lr}] = \begin{bmatrix} 0 \\ \vdots \\ 0 \end{bmatrix}_{N_l \times N_r}, \\ [M_{ll}] &= \begin{bmatrix} 2m_e & 0 & \cdots & 0 \\ 0 & \ddots & \ddots & \vdots \\ \vdots & \ddots & 2m_e & 0 \\ 0 & \cdots & 0 & m_e \end{bmatrix}_{N_l \times N_l}, \end{aligned} \quad (35)$$

$$\begin{aligned} [C_{rr}] &= [0]_{N_r \times N_r}, [C_{rl}] = [0 \quad \cdots \quad 0]_{N_r \times N_l}, [C_{lr}] = \begin{bmatrix} 0 \\ \vdots \\ 0 \end{bmatrix}_{N_l \times N_r}, \\ [C_{ll}] &= \begin{bmatrix} 0 & 0 & \cdots & 0 \\ 0 & \ddots & \ddots & \vdots \\ \vdots & \ddots & 0 & 0 \\ 0 & \cdots & 0 & c_d \end{bmatrix}_{N_l \times N_l}, \end{aligned} \quad (36)$$

$$\begin{aligned}
 [K_{rr}] &= [k_e]_{N_r \times N_r}, [K_{rl}] = [-k_e \quad 0 \quad \cdots \quad 0]_{N_r \times N_l}, \quad [K_{lr}] = \begin{bmatrix} -k_e \\ 0 \\ \vdots \\ 0 \end{bmatrix}_{N_l \times N_r}, \\
 [K_{ll}] &= \begin{bmatrix} 2k_e & -k_e & 0 & \cdots & 0 \\ -k_e & 2k_e & \ddots & \ddots & \vdots \\ 0 & \ddots & \ddots & -k_e & 0 \\ \vdots & \ddots & -k_e & 2k_e & -k_e \\ 0 & \cdots & 0 & -k_e & k_e + k \end{bmatrix}_{N_l \times N_l}.
 \end{aligned} \tag{37}$$

According to Eq. (34), we have

$$[M_{ll}]\{\ddot{U}_l^d\} + [C_{ll}]\{\dot{U}_l^d\} + [K_{ll}]\{U_l^d\} = -[M_{lr}]\{\ddot{U}_r^s\} - [M_{ll}]\{\ddot{U}_l^s\}. \tag{38}$$

Since the matrix $[C_{ll}]$ in Eq. (38) is not proportional to $[M_{ll}]$ and $[K_{ll}]$,²³ we introduce an identity equation²⁵ as follows:

$$[M_{ll}]\{\dot{U}_l^d\} - [M_{ll}]\{\dot{U}_l^d\} = \{0\}. \tag{39}$$

Combining Eqs. (38) and (39), we have

$$\begin{aligned}
 &\begin{bmatrix} [0] & [M_{ll}] \\ [M_{ll}] & [C_{ll}] \end{bmatrix} \begin{Bmatrix} \{\ddot{U}_l^d\} \\ \{\dot{U}_l^d\} \end{Bmatrix} + \begin{bmatrix} -[M_{ll}] & [0] \\ [0] & [K_{ll}] \end{bmatrix} \begin{Bmatrix} \{\dot{U}_l^d\} \\ \{U_l^d\} \end{Bmatrix} \\
 &= \begin{Bmatrix} \{0\} \\ -[M_{lr}]\{\ddot{U}_r^s\} - [M_{ll}]\{\ddot{U}_l^s\} \end{Bmatrix}.
 \end{aligned} \tag{40}$$

Equation (40) can be rewritten as the following form of state space for $\{y\}$:

$$[A]\{\dot{y}\} + [B]\{y\} = \{F(t)\}, \tag{41}$$

where

$$\begin{aligned}
 [A] &= \begin{bmatrix} [0] & [M_{ll}] \\ [M_{ll}] & [C_{ll}] \end{bmatrix}, \quad [B] = \begin{bmatrix} -[M_{ll}] & [0] \\ [0] & [K_{ll}] \end{bmatrix}, \quad \{y\} = \begin{Bmatrix} \{\dot{U}_l^d\} \\ \{U_l^d\} \end{Bmatrix}, \\
 \{F(t)\} &= \begin{Bmatrix} \{0\} \\ -[M_{lr}]\{\ddot{U}_r^s\} - [M_{ll}]\{\ddot{U}_l^s\} \end{Bmatrix}.
 \end{aligned} \tag{42}$$

Here, we consider the homogeneous equation obtained by setting the right-hand side of Eq. (41) to be zero

$$[A]\{\dot{y}\} + [B]\{y\} = \{0\}. \tag{43}$$

We assume the free-vibration solution to be

$$\{y\} = e^{\lambda t}\{\psi\}. \tag{44}$$

By substituting Eq. (44) into Eq. (43), we have

$$\lambda_i[A]\{\psi_i\} = -[B]\{\psi_i\}, \tag{45}$$

where $\{\psi_i\}$ and λ_i denote the i th complex-valued eigenmode and i th complex-valued eigenvalue, respectively.

Solving Eq. (41) by using the mode superposition method, we have

$$\{y(t)\} = [\Psi]\{z(t)\}, \tag{46}$$

where the modal matrix $[\Psi]$ is the collection of all the mode shapes $\{\psi_i\}$, and $\{z(t)\}$ is the column vector of the modal (or generalized) co-ordinates of the dynamic-inertia part. Substituting Eq. (46) into Eq. (41) and pre-multiplying by $[\Psi]^T$, we have

$$[\Psi]^T[A][\Psi]\{\dot{z}(t)\} + [\Psi]^T[B][\Psi]\{z(t)\} = [\Psi]^T\{F(t)\}, \tag{47}$$

where

$$[\Psi]^T[A][\Psi] = \begin{bmatrix} \ddots & & & \\ & a_i^* & & \\ & & \ddots & \\ & & & \ddots \end{bmatrix}, \tag{48}$$

where a_i^* is the diagonal element. Therefore, Eq. (47) can be reduced to

$$\dot{z}_i(t) - \lambda_i z_i(t) = \frac{1}{a_i^*} N_i(t), i = 1, 2, \dots, 2N_l, \tag{49}$$

where $N_i(t)$ is the i th element of $[\Psi]^T\{F(t)\}$. Finally, we obtain $\{z(t)\}$ by solving Eq. (49). Therefore, the vectors, $\{y(t)\}$ and $\{U_l^d\}$, are obtained. By adding the quasi-static part solution in Eq. (22), the total solution is obtained.

3. Illustrative Examples

For demonstration, a finite bar with an external viscous damper and a spring boundary subjected to a support motion is considered, as shown in Fig. 1. For simplicity, the model parameters are given: $c = 1\text{ m/s}$, $EA = 1\text{ N}$, $L = 7\text{ m}$, $c_d = 3\text{ N} \cdot \text{s/m}$ and $k = 5\text{ N/m}$. For simplicity, the support motion is specified by

$$a(t) = \sin(t). \tag{50}$$

Since this paper focuses on the analytical solution, geometry and material parameters are simply given in the numerical experiment. In engineering applications, real geometry size and true material parameters can be adopted. In addition, the reason

why we choose the sine function is to satisfy the I. C. of $u(x, 0) = 0, 0 \leq x \leq L$. The choice of only cosine function may contradict the I. C. To simulate the true input motion of an earthquake, superposition of sine and cosine functions can be applied, although numerical integral is required instead of an analytical solution.

3.1. General case ($c_d \neq 0, k \neq 0$)

The convergence test of FEM for the displacement is shown in Fig. 4. We find that when the number of nodes increases to 50, the displacement response obtained by the FEM matches well with the analytical solution obtained by using the diamond rule.

The displacement profile with the silent area for $t = 3$ and 5 s by using the diamond rule and the FEM are shown in Figs. 5(a) and 5(b), respectively. In Fig. 6(a), shadow regions, I and III, denote the dead zone. It matches the silent response obtained by the diamond rule which begins at $x = 3$ and 5 m to the end of the bar ($x = 7$ m), for the time of $t = 3$ and 5 s as shown in Fig. 5. It is found that the slope is discontinuous at $x = 3$ and 5 m for the time $t = 3$ and 5 s, respectively. These discontinuities occur at the location of (3,3) and (5,5) in the $x-t$ plane as shown in Fig. 6(a). As theoretically predicted, the discontinuity of the slope accurately occurs at the positions of (3,3) and (5,5), on the characteristic line.

Regarding the non-silent area, the displacement profile at $t = 8$ and 10 s is shown in Figs. 7(a) and 7(b), respectively. It is also found that the slope is discontinuous at $x = 6$ and 4 m for the time $t = 8$ and 10 s, respectively. These slope discontinuities

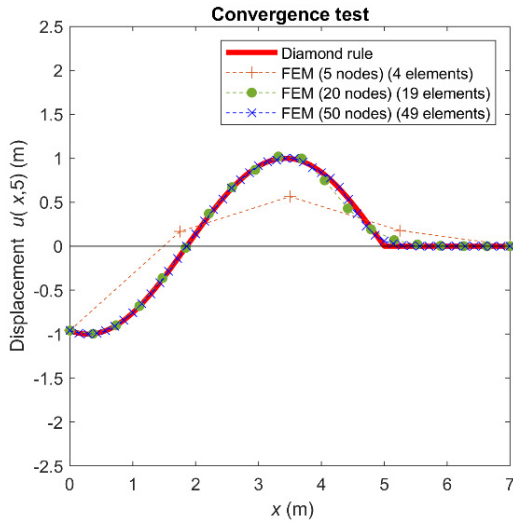


Fig. 4. Convergence test of the discrete system for $u(x, 5)$ ($c_d \neq 0, k \neq 0$).

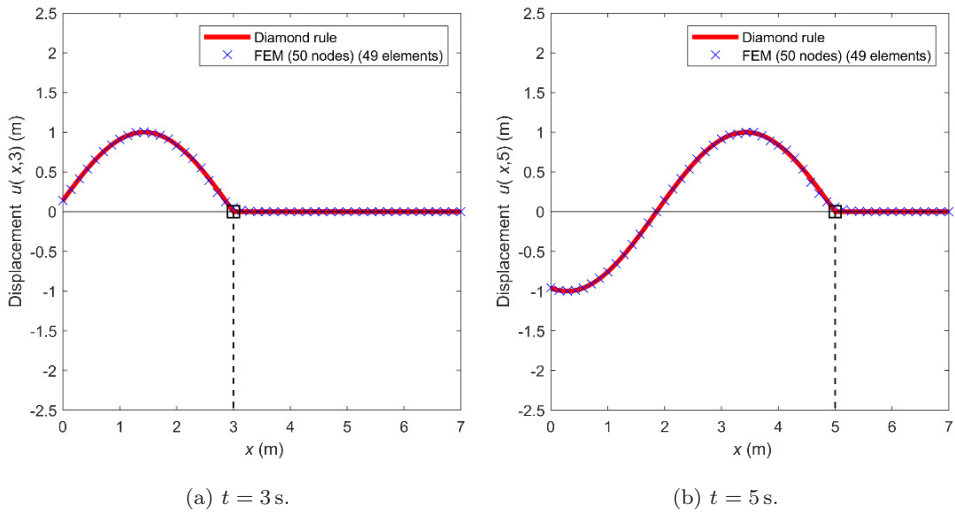
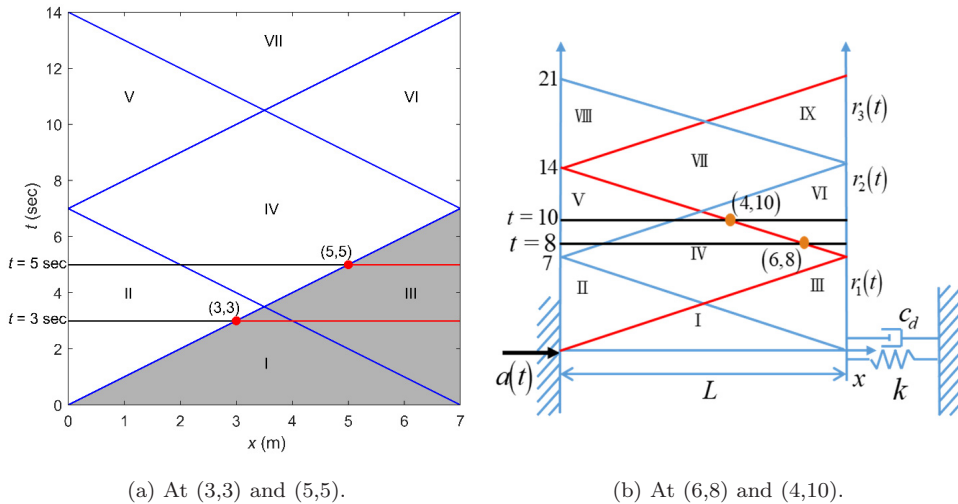


Fig. 5. Displacement profiles with the silent area by using the diamond rule and the FEM ($c_d \neq 0, k \neq 0$).



(a) At (3,3) and (5,5). (b) At (6,8) and (4,10).

Fig. 6. The locations of slope discontinuities on the characteristic lines.

occur at the location of (6,8) and (4,10) in the $x-t$ plane as shown in Fig. 6(b). This finding matches well with the mathematical requirement that the discontinuity can only occur at the position on the characteristic line.²⁶ In addition, the distribution of axial force at $t = 8$ s is shown in Fig. 8. It is found that the axial force is discontinuous at $x = 6$ m, and it corresponds to the slope of displacement at $x = 6$ m

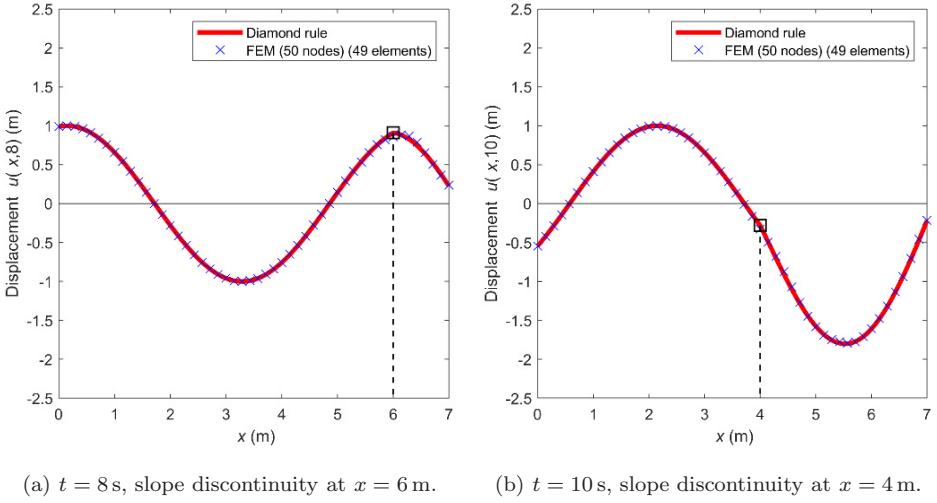


Fig. 7. Displacement profiles without the silent area by using the diamond rule and the FEM ($c_d \neq 0, k \neq 0$).

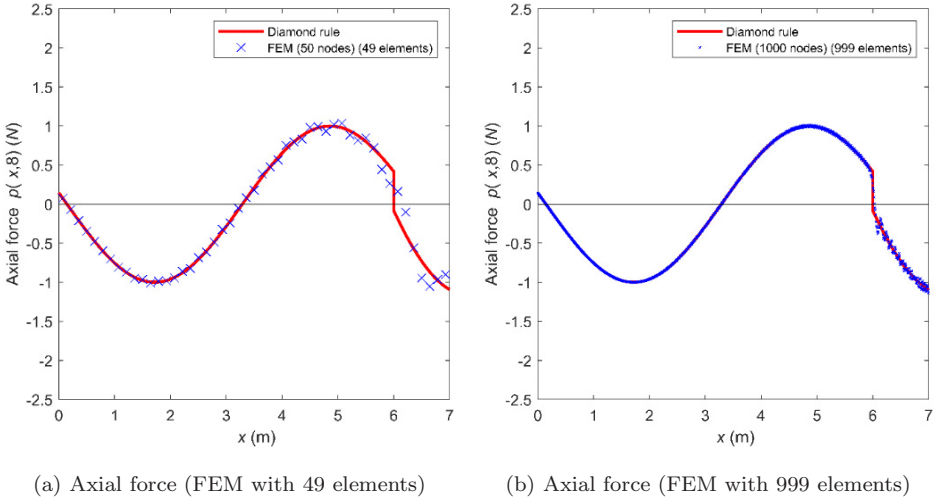


Fig. 8. Distribution of the axial force at $t = 8$ by using the diamond rule and the FEM ($c_d \neq 0, k \neq 0$) ($t = 8\text{ s}$).

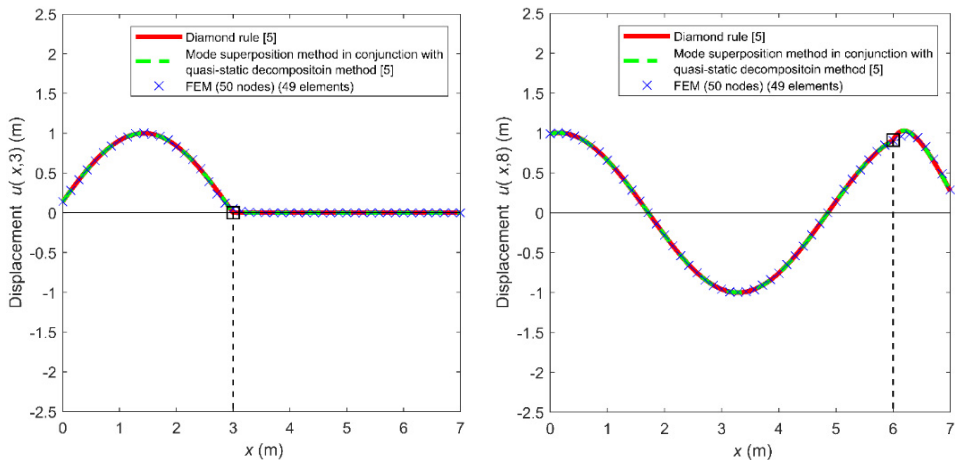
and the time $t = 8\text{ s}$ as shown in Fig. 7(a). It is straightforward to explain the displacement discontinuity at $(6,8)$ by plotting the distribution of axial force at $t = 8\text{ s}$. In Fig. 8, it is also found that the axial force by using the FEM needs more elements so that it can obviously show the discontinuity. In Fig. 8, the location of slope discontinuity of the non-quiet zone is also found on the characteristic line. According to the mathematical theory, the slope discontinuity of the displacement

curve only occurs on the characteristic line, no matter in the non-quiet or quiet zone. Physically speaking, the slope discontinuity occurs at the wave front of the support motion.

3.2. Two special cases ($c_d = 0$ or $k = 0$)

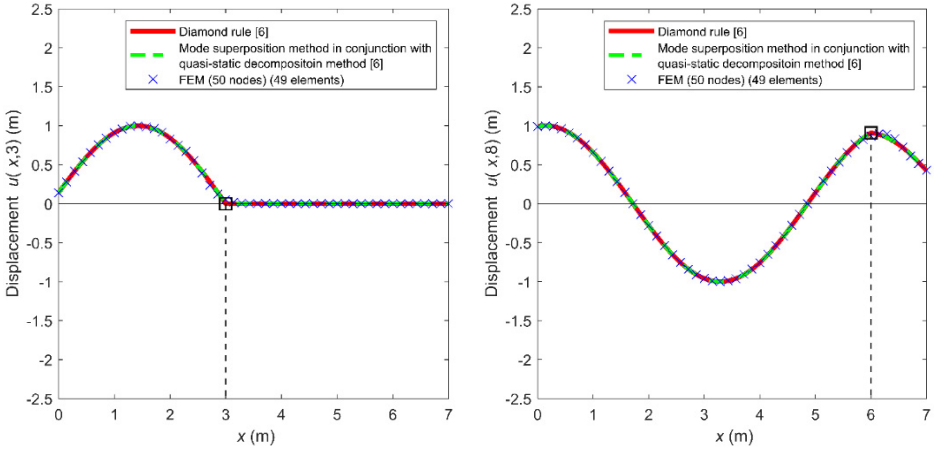
For two special cases, we employed the FEM to revisit the same problems of single spring⁵ and single damper,⁶ respectively, and obtain the agreeable results of analytical solutions.^{5,6} Here, we consider a special case where the damping coefficient is zero ($c_d = 0\text{ N} \cdot \text{s}/\text{m}$). In other words, only a spring on the right boundary. The result of FEM of this special case is also compared with that of the previous paper⁵ as shown in Fig. 9. The total displacement is compared with those obtained by using the mode superposition method in conjunction with the quasi-static decomposition method and the method of diamond rule used in the previous literature,⁵ as shown in Fig. 9. In this special case, the FEM result also shows the dead zone in Fig. 9(a). The FEM result matches the silent response which begins at $x = 3$ to the end of the bar ($x = 7\text{ m}$), for the time of $t = 3\text{ s}$, as shown in Fig. 9(a). Regarding the non-silent area for this only spring case, the displacement profile at $t = 8\text{ s}$ is shown in Fig. 9(b). In the same way, it is found that the slope is discontinuous at $x = 3$ and 8 m for the time $t = 3$ and 6 s , respectively. This outcome reconfirms that discontinuity occurs on the characteristic line.

Similarly, the other special case is considered where the spring constant is taken as zero ($k = 0\text{ N}/\text{m}$), namely only a viscous damper on the right-hand side. Likewise, the FEM result also can show the dead zone for this case, as shown in Fig. 10(a).



(a) Total displacement with the dead zone at $t = 3\text{ s}$. (b) Total displacement without the dead zone at $t = 8\text{ s}$.

Fig. 9. Special case for only spring ($c_d = 0, k \neq 0$).

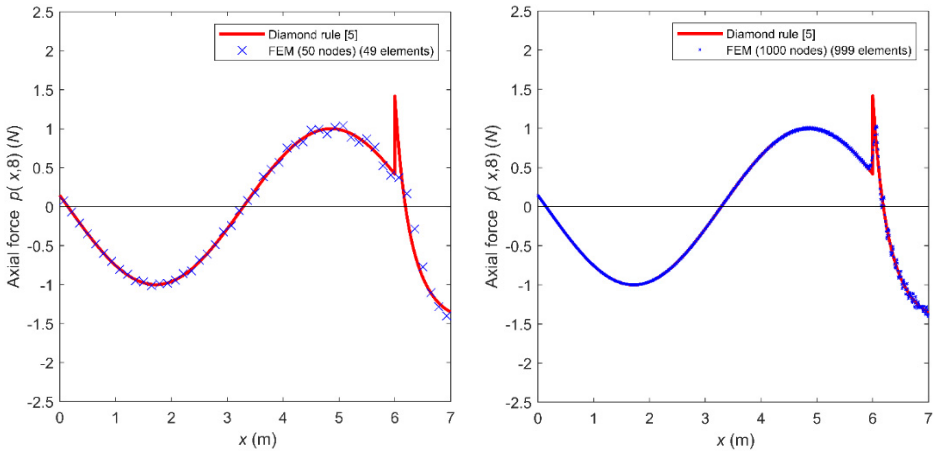


(a) Total displacement with the dead zone at $t = 8$ s. (b) Total displacement without the dead zone at $t = 8$ s.

Fig. 10. Special case of only damper ($c_d \neq 0, k = 0$).

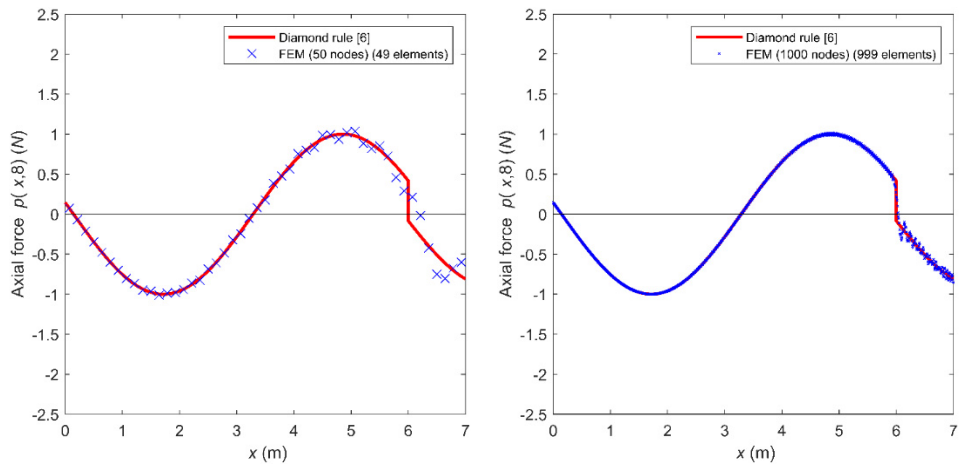
Regarding the non-silent area for this only damper case, the displacement profile at $t = 8$ s is shown in Fig. 10(b). It is also found that the slope is discontinuous at $x = 3$ and 8 m for the time $t = 3$ and 6 s, respectively.

The distribution of axial force for these two cases at $t = 8$ s is shown in Figs. 11 and 12. Similarly, the axial force of these two special cases by using the FEM needs more number of finite elements to show the obvious discontinuity.



(a) Axial force (FEM with 49 elements). (b) Axial force (FEM with 999 elements).

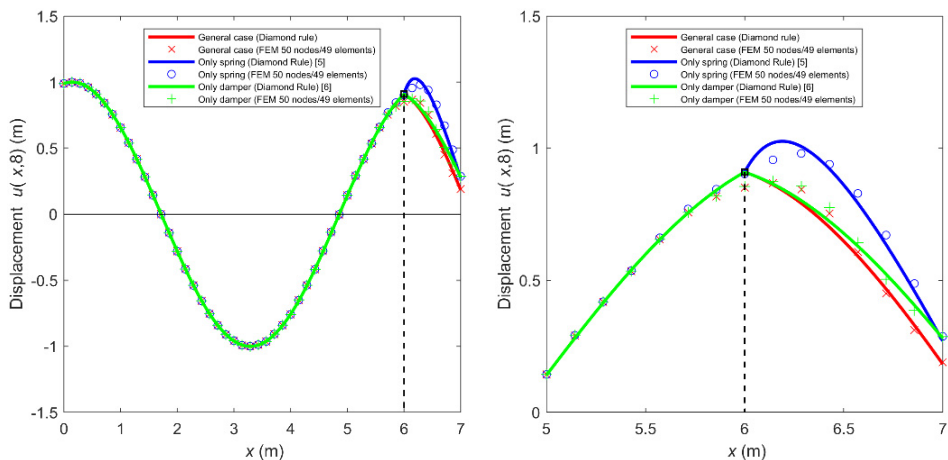
Fig. 11. Distribution of the axial force for the case of only single spring ($t = 8$ s).



(a) Axial force (FEM with 49 elements). (b) Axial force (FEM with 999 elements).

Fig. 12. Distribution of the axial force for the case of only single damper ($t = 8$ s).

It is interesting to find that Figs. 5(a), 9(a) and 10(a) show the same result of silent response even though they have different B.c.s. The physical interpretation is that the disturbance of support motion does not arrive at the right boundary. For $t = 10$ s, the reflection wave due to the boundary spring or damper has arrived. Therefore, the displacement profiles of the three cases are different, as shown in Fig. 13. In Fig. 13(a), no obvious difference from $x = 0$ to 6 is observed. However,



(a) Global displacement profiles. (b) Local displacement profiles.

Fig. 13. Displacement profiles for three cases (spring, damper and both) at $t = 8$ s.

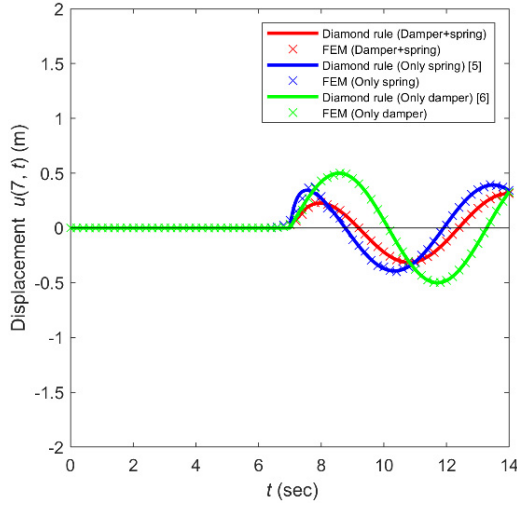


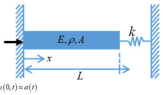
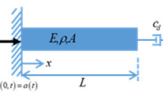
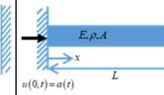
Fig. 14. Displacement history for three cases at $x = 7$ m by using the diamond rule and the FEM.

they deviate after $x = 6$ m since the boundary effect of a spring or a damper influences, as shown in Fig. 13(b). Nevertheless, all FEM results also match the phenomenon. The zoom view of the local displacement profiles for three cases is shown in Fig. 13(b). In Fig. 13, it is found that the displacement profile at $x = 6$ – 7 m of the general case with a damper and a spring boundary is smaller than the other two cases. Finally, the displacement response history of three cases at $x = 7$ m by using the diamond rule and FEM is shown in Fig. 14.

4. Conclusion

The support motion problem of a finite bar with a viscous damper and a spring on the boundary was successfully solved by using analytical and numerical methods. For the analytical and numerical methods, the method of diamond rule and the FEM were both independently employed to derive exact and numerical solutions, respectively. Our analytical approach to the method of diamond rule is both simple and feasible and is highly recommended to scientists and engineers since the duration of the support motion is short in an earthquake. For the method of diamond rule, the displacement response can be straightforwardly calculated in the space-time domain without considering the separation variables of space and time. Since the displacement solution was decomposed into two parts of quasi-static and dynamic-inertia solutions in the FEM, we only need a few numbers of degrees-of-freedom, such as 50 nodes (49 elements), to match well with the analytical solution. This can improve the efficiency of the computer computation. In addition, the FEM can also capture the dead zone or the so-called silent area in Figs. 5, 9(a) and 10(a). In two special

Table 1. Solutions of three cases by using different approaches.

Problem		Spring ($c_d = 0, k \neq 0$)	Damper ($c_d \neq 0, k = 0$)	Spring and damper ($c_d \neq 0, k \neq 0$)
				
Analytical solution	Diamond rule (method of characteristics)	Reference 5	Reference 6	Present
	Mode superposition method in conjunction with the quasi-static decomposition technique	Reference 5	Reference 6	NA*
Numerical solution	FEM	Present	Present	Present
Dead zone (silent area)		Present	Present	Present
Slope discontinuity occurring on the characteristic line		✓	✓	✓

Note: *NA: not available.


cases, three approaches including the mode superposition method in conjunction with the quasi-static decomposition technique, the method of diamond rule and the FEM yield agreeable results. Besides, it was observed that all slope discontinuities appeared on the characteristic line in Figs. 5, 7, 9 and 10, as theoretically predicted. It was observed that the displacement amplitude in the general case is smaller in comparison with the other two special cases in Fig. 13. This finding aligns with the practical application in engineering. However, the analytical result has not yet been derived for the general case in this paper by using the modal superposition method for the continuous system, since complex-valued eigenvalues and orthogonal relation cannot be expressed in an explicit form. Three cases are summarized in Table 1. Finally, this work can provide a benchmark example for comparison when other new analytical solutions are derived or other numerical solutions are developed.


Acknowledgments

The authors disclosed receipt of the following financial support for the research, authorship, and/or publication of this paper: Financial support from the National Science and Technology Council under Grant No. 110-2221-E-019-011-MY3 to

National Taiwan Ocean University was highly appreciated. We also appreciate NSTC-Taiwan support authors to present part results of this paper.

ORCID

Jeng-Tzong Chen  <https://orcid.org/0000-0001-5653-5061>

Jia-Wei Lee  <https://orcid.org/0000-0002-3336-8050>

References

1. G. Oliveto, A. Santini and E. Tripodi, Complex modal analysis of a flexural vibrating beam with viscous end conditions, *J. Sound Vib.* **200** (1997) 327–345.
2. A. J. Hull, A closed form solution of a longitudinal bar with a viscous boundary condition, *J. Sound Vib.* **169** (1994) 19–28.
3. R. Singh, W. M. Lyons and G. Prater, Complex eigensolution for longitudinally vibrating bars with a viscously damped boundary, *J. Sound Vib.* **133** (1989) 364–367.
4. J. T. Chen and Y. S. Jeng, Dual series representation and its applications a string subjected to support motions, *Adv. Eng. Softw.* **27** (1996) 227–238.
5. J. T. Chen, H. C. Kao, Y. T. Lee and J. W. Lee, Support motion of a finite bar with an external spring, *J. Low. Freq. Noise Vib. Act. Control* **41** (2022) 1014–1029.
6. J. T. Chen, H. C. Kao, J. W. Lee and Y. T. Lee, Support motion of a finite bar with a viscously damped boundary, *J. Mech.* **38** (2022) 473–490.
7. J. T. Chen, H.-K. Hong, C. S. Yeh and S. W. Chyuan, Integral representations and regularization for a divergent series solution of a beam subjected to support motion, *Earthq. Eng. Struct. Dyn.* **25** (1996) 909–925.
8. J. T. Chen, K. S. Chou and S. K. Kao, One-dimensional wave animation using Mathematica, *Comput. Appl. Eng. Educ.* **17** (2009) 323–339.
9. J. T. Chen, H.-K. Hong and C. S. Yeh, Modal reaction method for modal participation factors in support motion problems, *Commun. Numer. Methods Eng.* **9** (1995) 479–490.
10. L. Zhao and Q. Chen, Neumann dynamic stochastic finite element method of vibration for structures with stochastic parameters to random excitation, *Comput. Struct.* **77** (2000) 651–657.
11. Y. Ma and B. Wang, Analytical wave propagation method for free and forced transverse vibration analysis of a system of multiple elastically connected beams, *Int. J. Struct. Stab. Dyn.* **23**(15) (2023) 2350170.
12. E. L. Albuquerque, P. Sollero and P. Fedelinski, Free vibration analysis of anisotropic material structures using the boundary element method, *Eng. Anal. Bound. Elem.* **27** (2003) 977–985.
13. A. Amir, S. Saeid and A. Mojtaba, Free-Vibration, buckling, and static analysis of sandwich panels with a square honeycomb core using a meshfree method, *Int. J. Struct. Stab. Dyn.* (2023) 2450177, <https://doi.org/10.1142/S0219455424501773>.
14. L. X. Peng, X. C. He, G. X. Mei and Y. J. Shen, Dynamic response analysis of ribbed plate resting on viscoelastic pasternak foundation via MLS meshless method, *Int. J. Struct. Stab. Dyn.* (2023) 2450191, <https://doi.org/10.1142/S0219455424501918>.
15. V. Jovanovic, A Fourier series solution for the transverse vibration response of a beam with a viscous boundary, *J. Sound Vib.* **330** (2011) 1504–1515.

16. V. Jovanovic, A Fourier series solution for the transverse vibration of a clamped beam with a torsional damper at the boundary, *J. Vib. Control* **18** (2011) 344–356.
17. F. E. Udawadia, On the longitudinal vibrations of a bar with viscous boundaries super-stability super-instability and loss of damping, *Int. J. Eng. Sci.* **50** (2012) 79–100.
18. V. Jovanovic, A Fourier series solution for the longitudinal vibrations of a bar with viscous boundary conditions at each end, *J. Eng. Math.* **79** (2013) 125–142.
19. M. Gurgoze and H. Erol, Dynamic response of a viscously damped cantilever with a viscous end condition, *J. Sound Vib.* **298** (2006) 132–153.
20. S. J. Farlow, *Partial Differential Equations for Scientists and Engineers* (John Wiley & Sons, New York, 1982).
21. D. H. Wilkinson and E. M. Curtis, Water hammer in a thin walled pipe, in *Proc. 3rd Int. Conf. Pressure Surges*, Canterbury, England, March 1980, pp. 221–240.
22. F. John, *Partial Differential Equation*, 2nd edn. (Springer-Verlag, New York 1975).
23. S. Xing and J. Q. Sun, Multi-objective optimization of an elastic rod with viscous termination, *Math. Comput. Appl.* **27** (2022) 94.
24. S. Xin and J. Q. Sun, Impulse response of an elastic rod with a mass-damper-spring termination, *J. Vib. Test Syst. Dyn.* **7** (2023) 169–186.
25. W. C. Hurty and M. F. Rubinstein, *Dynamics of Structures*, 1st edn. (Prentice-Hall, New Jersey, 1964).
26. G. F. Carrier and C. E. Pearson, *Partial Differential Equations: Theory and Technique*, 1st edn. (Academic Press, New York, 1976).